Physica A 510 (2018) 208–218

Contents lists available at ScienceDirect

Physica A

journal homepage: www.elsevier.com/locate/physa

The influence of geometry on the elastic properties of the Drosophila wing disc

Arne Keller, Flavio Lanfranconi, Christof M. Aegerter*

Physik-Institut, University of Zurich, Winterthurerstrasse 190, 8057 Zurich, Switzerland

HIGHLIGHTS

- Concurrent 3D imaging and stretching of biological tissues.
- Finite element modeling of elastic properties of tissues.
- Description of elastic properties under direct consideration of the 3D structure.

ARTICLE INFO

Article history:
Received 20 March 2018
Received in revised form 16 May 2018
Available online xxxx

Keywords:
Biological tissue
Elasticity
Finite element
Drosophila
Force–displacement curve
Neo-Hookean

ABSTRACT

We consider the non-linear elastic behavior of the wing disc of the Drosophila larva. In stretching experiments, this epithelial tissue shows a highly non-linear force–displacement behavior. In order to understand the nature and origin of this non-linear reaction, we try to reproduce the deformation experiments using a two-dimensional finite element solution of the non-linear hyperelastic momentum balance equation. The results suggest that to a large extent the stress reaction of the tissue is due to purely geometric effects. Finally, we give a parameter estimate for a neo-Hookean constitutive model.

1. Introduction

The investigation of mechanical effects on developing tissues has recently gained increasing attention [1], ranging from the mechanisms of force generation in cell division [2], cell mobility [3], as well as tissue deformations on the scale of epithelia [4,5], and entire embryos [6–8], as well as the mechanical control of gene regulation [9,10] and growth [11–14].

In order to experimentally investigate the influence of forces in development, several types of force applications have been performed, most notably, laser ablation [4,8], but also theoretical inference of forces based on cell and/or tissue deformations [1,6,7]. Direct application of mechanical forces on tissues has also been performed, macroscopically [9,10,15] as well as microscopically by changing the activity of molecular motors [2,3]. However the extent of local force, which presumably is important in the biological effectiveness of control via mechanical forces, is difficult to quantify in these cases.

Here we study one such model system, namely the wing imaginal disc of Drosophila, a proto-organ inside the larva of Drosophila that will become the adult wing during pupariation. In this system, it has been shown theoretically [12–14] as well as experimentally [15,16] that mechanical forces are vital in the control of growth and size determination. In order to study molecular mechanisms at work in this control, as proposed in [14,16,17], forces need to be manipulated and quantified on the cellular level inside a live tissue. For this reason, we study the transmission of externally applied forces through the tissue,

* Corresponding author.
E-mail address: aegerter@physik.uzh.ch (C.M. Aegerter).

https://doi.org/10.1016/j.physa.2018.06.106

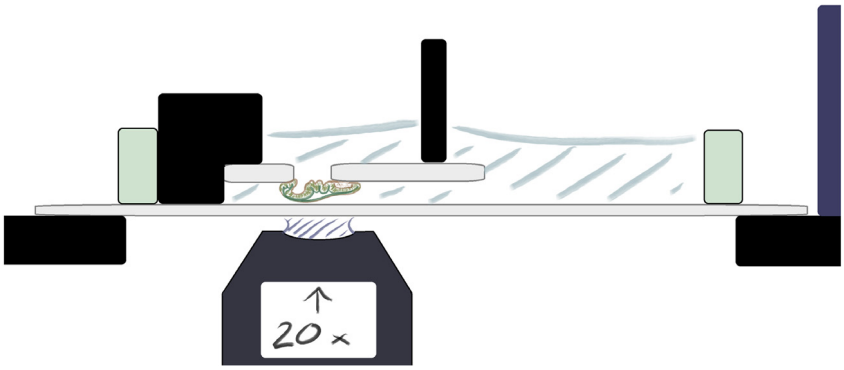

Fig. 1. Schematic of the stretching setup used in the experiments. Dissected wing imaginal discs are attached to cover slips using polylysine. One cover slip is moved with respect to the other while attached to a cantilever spring, whose deflection is measured in order to determine the applied force. The entire setup is mounted on a confocal microscope such that simultaneous three-dimensional microscopy and stretching are possible.

both experimentally and computationally. By determining the force extension curve of the tissue simultaneously with the three-dimensional structure deformation, we are able to disentangle the influence of geometry and the material on the stress inside the tissue at different applied forces. For this purpose, we use the structural information from the three-dimensional imaging and propose a material model, which is then solved using finite elements and compared with the experimental force extension curve as well as the experimental deformation. Using a linear hyperelastic model for the material, with a stiff layer surrounding the tissue corresponding to the extra-cellular matrix, we can describe the highly non-linear force extension curve to a reasonable approximation, while also capturing the structural changes in the overall folded tissue as a result of the stretching. With this we obtain a map of the stress-distribution inside the tissue for a given applied force. This information can be put back into studies of the influence of forces on development on the cellular level, since this allows the quantification of forces at specified positions given an external perturbation.

2. Experiments

2.1. Setup

The experimental setup used to apply a quantitatively determined force onto a wing disc is similar to that described in [18]. The wing discs are dissected and immediately inserted to a special stretching apparatus, where the wing disc is attached to two independently moving cover slips while submerged in a nourishing medium [19]. The stretching is applied by moving one of the cover slips, while keeping the other fixed, and the applied force being determined from the bending of a cantilever spring attached to the movable cover slip. This is shown schematically in Fig. 1. The dimensions of the cantilever as well as the accuracy in the positioning of the cover slip allow a controlled application of forces ranging between 1 μN and 300 μN. The stretching apparatus is mounted on top of an inverted Leica SP1 confocal microscope, allowing for the concurrent determination of the three-dimensional structure of the wing disc tissue, as well as in principle a concurrent determination of cell shapes using appropriate fluorescent markers [20]. With this setup, we can measure force–displacement curves, while simultaneously determining the three-dimensional structure of the tissue as well as the extra-cellular matrix, with a particular emphasis on the dynamics of the folds in the tissue during stretching.

2.2. Experimental results

Fig. 2 shows an example of a wing disc stretching experiment, where the shape of the wing disc in two perpendicular cross-sections is shown at different levels of stretching (0, 1, 14, 21 μN respectively). The wing discs investigated have been marked fluorescently by live markers of Lac:YFP (shown in green) and TROL:GFP (shown in red), thus showing the epithelial cells (Lac:YFP) as well as the extra-cellular matrix (TROL:GFP). Where the two channels overlap, the figure shows yellow. As can be seen, already a very small force of 1 μN leads to a considerable extension of the wing disc of 80 μm, indicating a very soft material. For further extensions however, considerably higher forces are necessary. This indicates a highly non-linear shape of the force extension curve, which is shown in Fig. 3. The geometry of the tissue shown in Fig. 2 shows a visible unfolding of the outer layer of the wing disc during the initial stages of the stretching, whereas at higher forces, the outer layer, consisting mainly of the extra-cellular matrix, is flat and stretched tight.

From these results, it seems that the highly non-linear elastic behavior of the wing disc tissue is rather not a material property, but merely an effect due to the unfolding of the geometry of the structure. In the following, we will investigate this question more closely with the help of a numerical model, which is fed with an assumption on the constitutive behavior, and calculates the deformation behavior and the stress distribution as a result. In consequence, it can be tested whether even

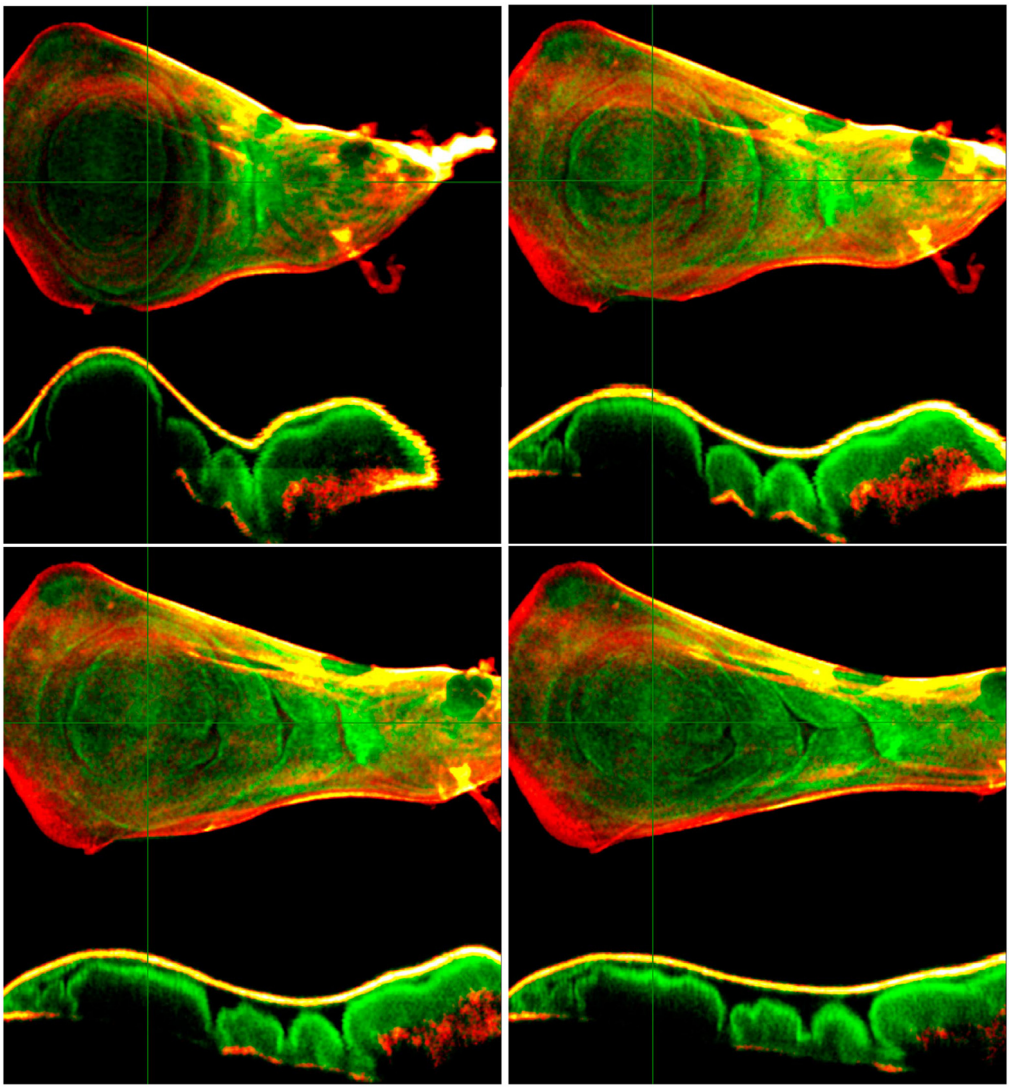

Fig. 2. Deformation experiment, microscopy images of 0 μm (top left), 30 μm (top right), 50 μm (bottom left) and 70 μm deformation of fixed boundary. (For interpretation of the references to color in this figure legend, the reader is referred to the web version of this article.)

with a very simple material behavior such as linear elasticity (or a large deformation framework that mimics linear elasticity as well as possible) can lead to such a highly non-linear force extension curve.

3. Numerical model

Typically, engineering materials are tested in the laboratory for their material properties. In order to do so, they are sampled in simple geometries and subjected to controlled deformations or stresses, while measuring the respective other. The results are compared to theoretically expected functional dependencies, allowing to calibrate a constitutive model and the corresponding phenomenological constants.

Such a procedure cannot easily be applied to naturally grown wing disc epithelia — any such transformation would kill the living cells constituting the tissue and hence change the properties of interest. Therefore, the special geometry of the sample has to be taken into account in the investigation. The momentum balance equation subject to the respective constitutive framework thus has to be solved numerically.

3.1. Constitutive model

During the deformation experiments, strains are in the order of magnitude of 1. A suitable constitutive model therefore must be capable of handling large deformations, together with the conceptual difficulties they induce to the kinematics

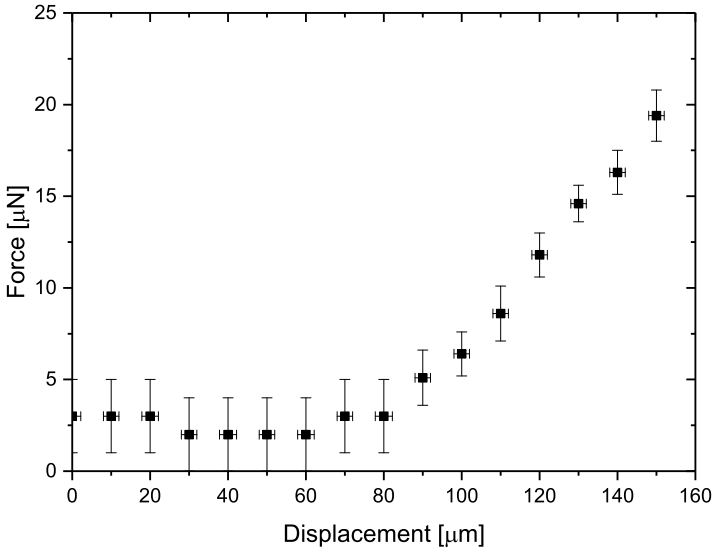

Fig. 3. Force extension curve averaged over nine subsequent extensions. The force extension curve is highly non-linear with a strong increase in its slope at an extension of roughly 80 μm, where the overall response stiffens by at least an order of magnitude. The fact that the extension returns to zero when the force is reduced indicates that the tissue reacts elastically on the time scale of the experiment, which is 900 s. The error bars correspond to standard deviations of the experimental curves.

of elasticity. Nevertheless, we would like to avoid using a highly non-linear constitutive model, which might over-fit the observed behavior due to a large number of parameters. Therefore, in the following we will consider a neo-Hookean elastic model [21], which mimics the behavior of linear elasticity within a hyperelastic framework to cope with large deformations. We choose this approach even though other authors successfully applied highly non-linear (such as exponential) elastic models [22] to living tissues, as we would like to focus on geometry-driven effects. After all, most non-linear stress–strain relations contain a neo-Hookean-like behavior as a limiting case for smaller deformations.

3.1.1. Momentum balance

In order to obtain governing equations for the reaction of any given continuum system, it is useful to consider balance equations for the conserved quantities of classical mechanics. The most important of these is linear momentum. Its balance reads as follows:

$$\frac{\mathrm{d}\mathbf{p}}{\mathrm{d}t} = \nabla \cdot \boldsymbol{\sigma} + \mathbf{f}, \tag{1}$$

where the left-hand side is the convective time derivative of the linear momentum density $\mathbf{p}$, and $\boldsymbol{\sigma}$ the Cauchy stress tensor. The bulk force density $\mathbf{f}$ can be neglected for our purposes — so can in a static–elastic situation the time derivative on the left-hand side. That is, the momentum balance **within** the material reduces to

$$\nabla_i \sigma_{ij} = 0, \tag{2}$$

where in order to illustrate the meaning of the divergence in Eq. (1) we have used Cartesian coordinate indices $i, j \in \{1, 2, 3\}$. The Cauchy stress tensor can in most cases not be inferred from first principle physics, and thus has to be postulated as a phenomenological constitutive relation. In a purely elastic setting, this relation is a function of only the momentary deformation of the material — a stress–strain relation.

3.1.2. Stress–strain relation

To close the system Eq. (1), we have to specify the Cauchy stress $\boldsymbol{\sigma}$ as a function of kinematic quantities. In a purely elastic setting, this means that $\boldsymbol{\sigma}$ has to be a function of the current state of deformation (and not its time derivatives). The idea of hyperelasticity is, furthermore, to write the Cauchy stress as a derivative of a strain energy potential, which, in turn, depends on a frame invariant strain measure. In order to construct the latter, let X_A be Cartesian coordinates of a reference configuration, and $x_i(t)$ those of the present configuration at a time t. The deformation gradient is defined as

$$F_{iA} = \frac{\partial x_i\,(X_A, t)}{\partial X_A}. \tag{3}$$

As a suitable strain measure we use the right Cauchy–Green deformation tensor,

$$C_{AB} = F_{iA} F_{iB}. \tag{4}$$

The neo-Hookean strain energy potential in a non-volume preserving version,

$$W = \frac{1}{2}a\left[\mathrm{tr}(\boldsymbol{C}) - 2\log J - 3\right] + \frac{1}{2}b\left(\log J\right)^2, \tag{5}$$

where $J = \det \mathbf{F}$, and $a,\ b$ are two phenomenological constants. The Cauchy stress tensor can be calculated as a derivative of the strain energy potential,

$$\sigma_{ij} = J^{-1}F_{iA}\frac{\partial W}{\partial F_{jA}} = aJ^{-1}\left(F_{iA}F_{jA} - \delta_{ij}\right) + bJ^{-1}\log J\delta_{ij}. \tag{6}$$

If we define the strain tensor $\boldsymbol{\varepsilon} = \frac{1}{2}(\nabla\mathbf{u} + \nabla\mathbf{u}^T)$ as the symmetric gradient of the displacement $\mathbf{u} = \mathbf{x} - \mathbf{X}$, an expansion to first order in the strain yields

$$\sigma_{ij} = 2a\,\varepsilon_{ij} + b\,\mathrm{tr}\boldsymbol{\varepsilon}\,\delta_{ij}. \tag{7}$$

That is, the constants $a,\ b$ for small strains agree with the Lamé parameters $\lambda,\ \mu$ commonly used in linear elasticity. The physical interpretation of these parameters is thus given by the behavior in the linear elasticity limit.

3.2. Plane strain approximation

For the sake of computational ease and in order to make use of the experimental information about the geometry of the wing disc, we restrict our theoretical considerations to a two-dimensional numerical model. In consequence, we have to project the three-dimensional physics into two dimensions. This – not necessarily trivial – task is done in a plane strain approximation, which assumes that the sample is symmetric on an axis perpendicular to the modeling plane. Even though this is certainly not the case, we argue that the main stretching axis is still along the model plane, and that probably a plane strain approximation is the most appropriate way of projecting the problem under consideration into two dimensions. We thus consider the displacement field $\boldsymbol{u}$ to be essentially limited to the two-dimensional $x-y$-plane, i.e. to be of a structure

$$\boldsymbol{u} = \begin{pmatrix} u_x \\ u_y \\ 0 \end{pmatrix} \tag{8}$$

in a suitably chosen coordinate system. Furthermore, all quantities only vary as a function of x and y (translational symmetry with respect to z).

In the linear elasticity limit, it is straightforward to show that the Cauchy stress tensor has the block diagonal structure

$$\boldsymbol{\sigma} = \begin{pmatrix} \sigma_{xx} & \sigma_{xy} & 0 \\ \sigma_{xy} & \sigma_{yy} & 0 \\ 0 & 0 & \sigma_{zz} \end{pmatrix}. \tag{9}$$

Furthermore, it is straightforward to show that for the two-dimensional stress,

$$\boldsymbol{\tau} = \begin{pmatrix} \sigma_{xx} & \sigma_{xy} \\ \sigma_{xy} & \sigma_{yy} \end{pmatrix}, \tag{10}$$

formally the same stress–strain relation applies as for the Cauchy stress $\boldsymbol{\sigma}$. That is, in a two-dimensional plane strain model, the constitutive relations can directly be "copied" from the 3D case, which gives this approximation a particular elegance. We calculate thus the two-dimensional stress tensor $\boldsymbol{\tau}$ using the framework pointed out in Eq. (6), while simply using the two-dimensional deformation gradients.

3.3. Geometry and boundary conditions

The two-dimensional physics now being set, we have to think about the actual geometry to model. As we aim at numerically studying the experiments pointed out in Section 2, we use a geometry measured optically in the beginning of an deformation experiment. The measured and mesh geometries are shown in Fig. 4.

As boundary conditions, we assume the outside surface to be moving freely, while on the inside cavity a constant pressure p is applied. This pressure could be adapted in a way to manipulate or keep constant the cavity volume. Nevertheless, it turned out that the influence of the pressure on the force–deformation results is very limited. We therefore set it to a value that is convenient for numerical stability and keep it constant throughout the whole numerical deformation experiment. The surface pressure is taken into account with a von-Neumann boundary condition

$$\boldsymbol{\tau}(\boldsymbol{x})\cdot\boldsymbol{n} = -p\boldsymbol{n},\ \boldsymbol{x}\in\mathcal{S}_p \tag{11}$$

on the pressure boundary surface $\mathcal{S}_p$, where $\boldsymbol{n}$ is a unit surface normal vector.

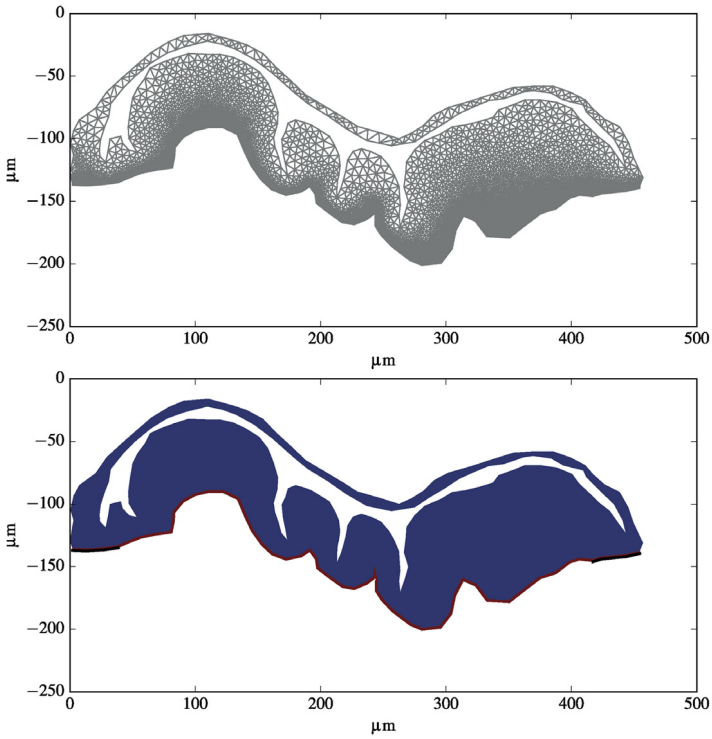

Fig. 4. The geometry of the finite element mesh. X and y axes: Position in µm. For the sake of visibility of elements, the coarsest mesh in use (14754 elements) is shown. Most of the results have been obtained with refined versions with 56818 and 230286 elements, where simply the edges of the shown mesh have been split. The bottom figure shows the layered structure of the model, with the body in blue and the extracellular matrix layer in red. The fixed parts of the boundary are marked in black. (For interpretation of the references to color in this figure legend, the reader is referred to the web version of this article.)

The external forcing in the stretching experiment is modeled by a Dirichlet boundary condition imposed on the displacement field $\boldsymbol{u}$,

$$\boldsymbol{u}(\boldsymbol{x}) = \begin{cases} 0, \ \boldsymbol{x} \in \mathcal{S}_0 \\ \boldsymbol{u}_0, \ \boldsymbol{x} \in \mathcal{S}_{\text{fix}}, \end{cases} \tag{12}$$

where $\mathcal{S}_0$ and $\mathcal{S}_{\text{fix}}$ are the respective parts of the surface where zero or a fixed displacement are imposed (as depicted in Fig. 4b). The response (i.e., the forces resulting from the applied displacement) is calculated from the modeled stress distribution on the Dirichlet surface. These boundary conditions mimic the experimental setup, where the displacement is the parameter that can be manipulated – even though for practical reasons the displacement has to be regulated to produce a certain force.

3.4. Layers

The epithelium tissue of the Drosophila wing disc constitutes an inhomogeneous material: even if we decide to ignore the presence of cells, the tissue is surrounded by an extracellular matrix, which consists of harder material than bodies of the cells. It is not very surprising that this plays a role for the elastic behavior of the structure. In order to investigate this, while constructing a finite element discretization of the chosen geometry, we implement different meshes allowing the model parameters a, b to vary locally; more precisely, we define a layer within the model geometry where the parameters are by a defined factor larger than in the rest of the tissue. The different layers are shown on the bottom of Fig. 4. This is considered a model for the effect of an extracellular matrix on the overall elastic behavior.

3.5. Numerical solution

The non-linear model equations with the boundary conditions pointed out in the previous section now have to be solved on the geometry given above. This is done in the open source Dolfin–FEniCS finite element framework [23]. An unstructured mesh is constructed as shown in Fig. 4, where the mesh resolution is particularly fine on the layer which corresponds to the extracellular matrix. The non-linear physics is solved with a Newton iteration, which usually converges after 10 to 30

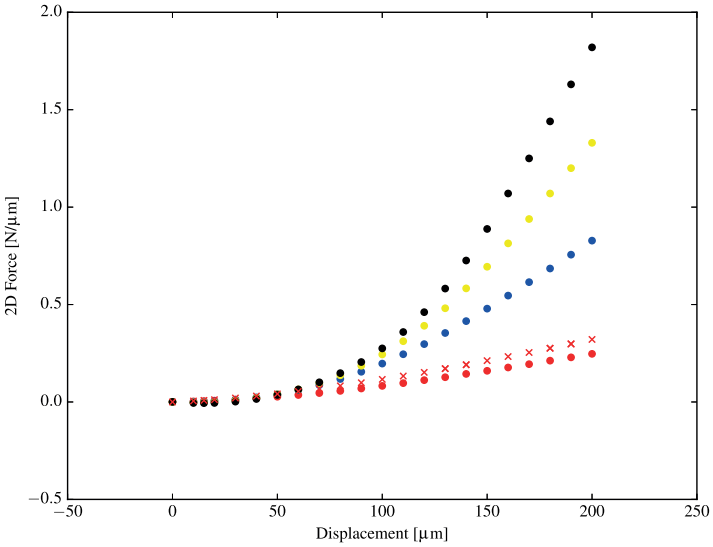

Fig. 5. Force–displacement curves with softening factors $E = 1$ (red), $E = 50$ (blue), $E = 100$ (yellow) and $E = 150$ (black). Additionally, a curve with a 100 times harder apical side (red crosses) is shown. (For interpretation of the references to color in this figure legend, the reader is referred to the web version of this article.)

iterations. In order to avoid discretization artifacts, a series of increasingly fine meshes is considered. This procedure proves successful even for very large deformations (strains up to 100% and more). As a result, the displacement field $\boldsymbol{u}(\boldsymbol{x})$ is obtained, from which the two-dimensional stress tensor field $\boldsymbol{\tau}(\boldsymbol{x})$ can be calculated by interpolation, and from this, in turn, the forces on the fixed surface $\mathcal{S}_{\text{fix}}$.

3.6. Fit procedure for elastic parameters

The elastic model parameters in Eq. (6) have to be determined by fitting model results to experimental values. This task is complicated by two issues: First, solving a finite element problem to a decent resolution is computationally intensive, making it difficult to run an optimization procedure which would require many model runs. Second, the two-dimensional model results have to be compared to three-dimensional experimental values, requiring a reasonable scaling.

In order to cope with those problems, we assume that the three-dimensional and two-dimensional forces scale as

$$F_{3D} = F_{2D}\, w_s, \tag{13}$$

where w_s is the width of the sample (roughly 200 µm). In order to simplify the fit, we introduce an additional dimensionless fit parameter in this equation,

$$F_{3D} = F_{2D} \cdot w_s f_{\text{fit}}. \tag{14}$$

The parameter f_{fit} can now be used for a least-squares fit of the modeled forces to the experimental result. Afterwards, the nonlinear nature of the numerical model requires running it again with elastic parameters adjusted according to the fit results, repeating the fit procedure until f_{fit} equals 1. This iteration avoids a costly probing of the model parameter space, while still tuning the model to the experimental results.

4. Model results

We run numerical simulations of the deformation experiment described in Section 3 in different model configurations. The primary aim of these model runs is to investigate whether the experimentally observed elasticity behavior can actually be captured by a two-dimensional model. Furthermore, we would like to obtain estimates of the material properties, i.e., numerical values for the constants of the constitutive model proposed in Section 3.1. Finally, we are interested in the influence of material inhomogeneities such as an extracellular matrix on the overall elastic behavior of the wing disc.

As shown in Fig. 4, the layered geometry is meshed with different resolutions. On those meshes, values for the elastic parameters a and b are fixed. They are either constant everywhere, or by an enhancement factor E larger on the extracellular matrix layer. This setup is then solved with a prescribed fixed displacement value u_0 on the fixed boundary part (see Fig. 7). A series of increasing values for u_0 ranging from 0 to 300 µm mimic the stretching experiments carried out experimentally.

Fig. 5 shows the resulting force–displacement curves for different model setups, i.e., different values of the hardening factor E, ranging from 1 to 150, 1 being equivalent to the absence of an extracellular matrix. The force values are still the

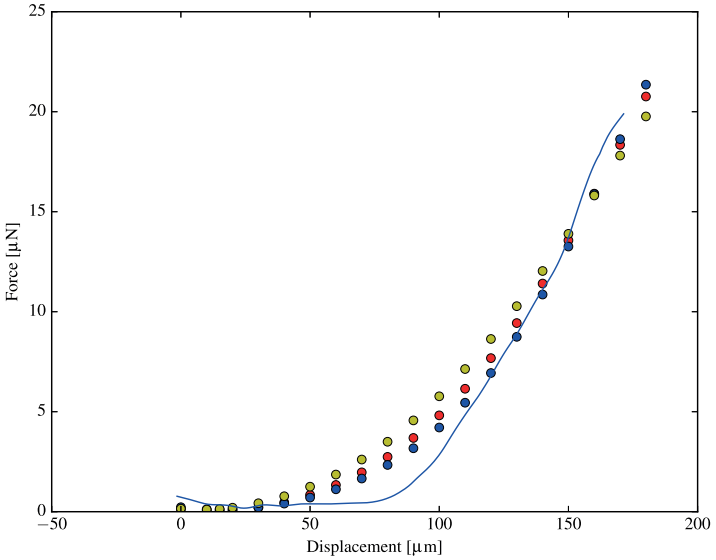

Fig. 6. Force–displacement curves for softening factors $E = 100$ (red dots) and $E = 50$ (blue dots), after fit. Solid line: experimental force results. (For interpretation of the references to color in this figure legend, the reader is referred to the web version of this article.)

Table 1
Parameters used for the three model runs with different values of the harening factor E.

Hardening factor	$E = 50$	$E = 100$	$E = 150$
Parameter			
a [kPa] on extracellular matrix	55(2)	$1.10(3) \cdot 10^2$	$1.65(3) \cdot 10^2$
b [kPa] on extracellular matrix	$1.07(4) \cdot 10^2$	$2.13(5) \cdot 10^2$	$3.20(6) \cdot 10^2$
a [kPa] on wingdisc body	1.10(4)	1.10(3)	1.10(2)
b [kPa] on wingdisc body	2.13(8)	2.13(5)	2.13(4)

two-dimensional forces F_{2D}, which have not been tuned to fit the experimental results yet. The influence of the harder layer representing the extracellular matrix can clearly be seen here. At $E = 1$, which corresponds to a homogeneous material (i.e., no extracellular matrix), the behavior is nearly linear; opposed to that, the higher E gets, the more the two-fold nonlinear behavior similar to the one observed experimentally is visible. Furthermore, in order to check influences due to the discretization, we calculated force–displacement curves with increasing mesh refinement, showing excellent convergence already with low mesh resolution.

As pointed out in Section 3.6, these results have to be fitted to match the experimental result. This is shown in Fig. 6. Some of the curves from Fig. 5 are now compared to the experimentally obtained force–displacement results. It turns out that particularly the model configuration with a 2 μm thick extracellular membrane and $E = 150$ matches the experimental results fairly well ($R^2 = 0.988$), but also the other configurations perform well with only slightly worse goodness of fit measures ($R^2 = 0.981$ and 0.957 for the $E = 100$ and the $E = 50$ configurations, respectively. The corresponding values for the model parameters a, b are assembled in Table 1. Additionally, in Fig. 5, results with a 100 times harder layer of 2 μm thickness on the *upper* side (cf. apical side, towards the cavity) of the wing disc body are shown. Interestingly, it turns out that these are not able to produce an elastic behavior any similar to the experimental results.

Apart from the force–displacement curves, we can also study the geometric behavior of the sample during the deformation experiment — which is particularly interesting in comparison with the experimental results shown in Fig. 2. When looking at the corresponding model results (Fig. 7), on the first glance the most striking feature is the top part of the structure "breaking" through the rest. This is a model artifact which would be comparably complicated to fix — a collision detection algorithm would have to be implemented for that. However, we can argue that at least for the configurations with an extracellular matrix, the top layer consist of very soft material compared to the rest of the structure. Therefore, it is not expected that it has a significant influence on the force–displacement curves.

Furthermore, when looking at the bottom side of the structure, it is clearly visible how the harder layer corresponding to the extracellular matrix is being flatted out. This flattening happens when the fixed boundary reaches a displacement around 80 μm, which is approximately when the steepening of the force–displacement curve appears. The stress distribution (color coded in the images) shows that the stresses are completely concentrated in this layer — that is, the force–displacement behavior is mainly influenced by the processes taking places here.

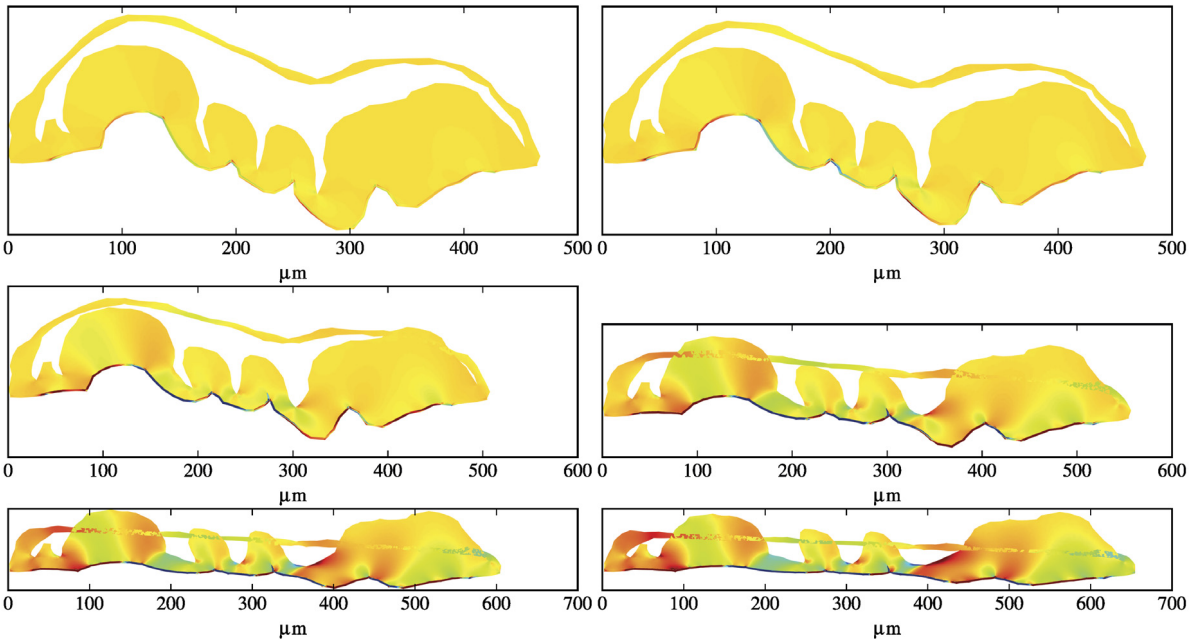

Fig. 7. Modeled deformation history: color coded is the shear component σ_{xy} of the Cauchy stress tensor. The color scale varies from −0.03 MPa (blue) to 0.015 MPa (red). Similar plots of the diagonal components can be found in the appendix. (For interpretation of the references to color in this figure legend, the reader is referred to the web version of this article.)

5. Discussion

From the qualitative comparison of model and experimental results it seems that – in spite of its two-dimensional nature – the numerical model can capture the most remarkable features of the strain behavior of the wing disc. Furthermore, we are able to infer numerical values for the model parameters (that is, in the limit of low strains, the Lamé parameters of linear elasticity). The modeled force–displacement curves manage to mimic the two-step (soft-hard), highly non-linear behavior observed experimentally, even though the non-linearity in the elastic behavior is not quite as pronounced as in the experiment. Furthermore, Fig. 7, shows that at large applied stress, these forces are acting mostly in the extracellular matrix.

The constitutive framework used in the model is that of neo-Hookean elasticity. As a large deformation generalization of linear elasticity, this theory is inherently non-linear, but only to an extent necessary to cope with large strains. Therefore, the highly non-linear shape of the force–displacement curves cannot be considered a particularity of the constitutive model — it is rather a geometric effect. Furthermore, it is only visible in the presence of a harder layer (modeling the extracellular matrix), which shows the important influence of the latter on the overall elastic behavior of the wing disc. This finding is further corroborated by the targeted dissolving of the actin network using latrinculinB in the main tissue. With this, any active force response in the mostly apical side of the main tissue is destroyed and its influence can be neglected. Carrying out this experiment does not change the overall elastic behavior [20], showing that the main response is due to something different from the actin network, leaving the extracellular matrix is as the most obvious candidate.

As visible on the pictures in Fig. 2, the wing disc is a complex three-dimensional structure, and it is therefore on the first look doubtful, whether the deformation of this structure can realistically be captured by a two-dimensional numerical model. This is certainly a weakness of the model presented here – particularly the estimates for the model parameter suffer from this problem, as their calculation relies on a plane strain projection. Nevertheless, the success of the two-dimensional model to reproduce important features of the experimental findings makes us optimistic that this approach at least helps to understand the nature of the elastic behavior, and to identify the importance of material inhomogeneities.

In spite of the findings and conclusions that can already be inferred from this two-dimensional numerical model, applying a three-dimensional model would be the obvious next step in order to gain further insights to the biomechanics of the drosophila wing disc. However, this task is trickier than it seems at the first glance. On the computational side, solving a full 3D hyperelasticity model is somewhat more costly, but feasible (suitable numerical methods are readily implemented in many available finite element packages, also in the FEniCS/Dolfin package used in this work). Experimentally, the situation is more complicated though: obtaining a suitable three-dimensional geometry and a corresponding finite element mesh of the wing disc from microscopy data is rather difficult. As during the stretching experiment the wing disc is imaged only from one side, the data quality is varying significantly on different sides of the structure. Whereas in 2D it is rather easy to extract

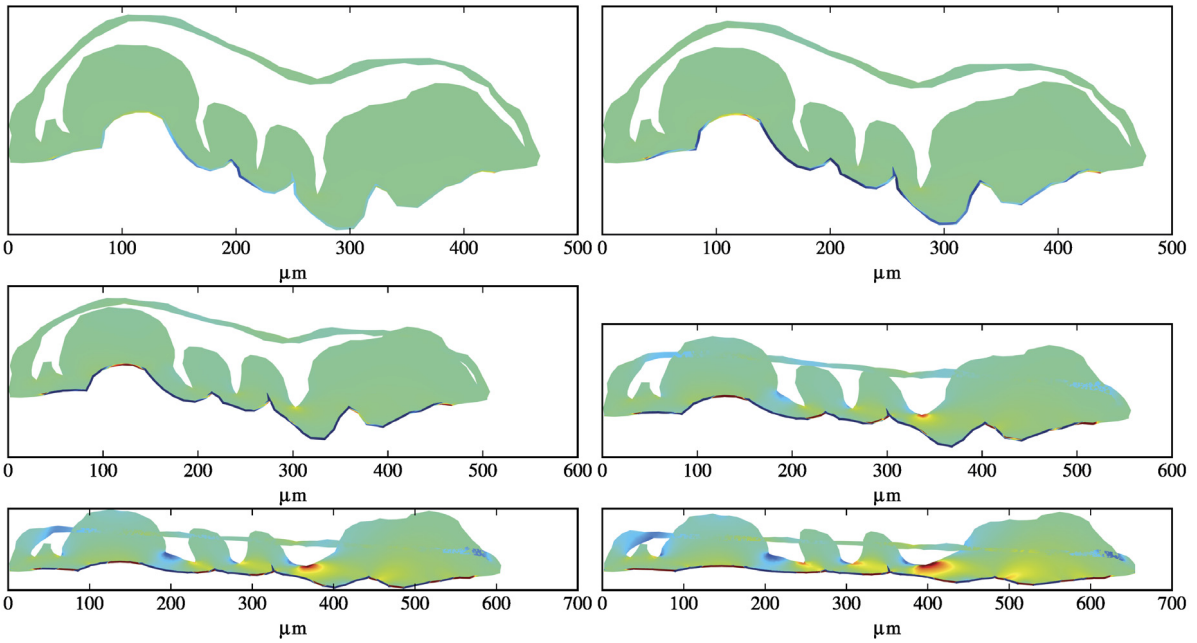

Fig. 8. Modeled deformation history: color coded is the horizontal component σ_{xx} of the Cauchy stress tensor. The color scale varies from −0.04 MPa (blue) to 0.045 MPa (red). (For interpretation of the references to color in this figure legend, the reader is referred to the web version of this article.)

a suitable geometry and mesh from those medium-quality images, obtaining a 3D mesh of the whole surface with neither geometric artifacts nor wholes due to lack of data is a highly non-trivial task. This turned out to be beyond the scope of what was technically feasible within this work, so we are leaving this as a challenge to future research.

6. Conclusion

In this work, we have presented laboratory measurements and a numerical model of elastic deformations of the Drosophila larva wing imaginal disk. The measured force–displacement curves show a very strongly non-linear behavior with a very soft start and a transition to a harder but asymptotically linear behavior for larger deformations. Microscopic images taken during the deformation experiments give reason to believe that a harder layer (extracellular matrix) on the outside of the structure, initially folded and unfolding during the deformation, plays a role for this behavior.

A two-dimensional finite element model of neo-Hookean elasticity, solved on a geometry designed according to imaged cross sections of the experimental sample, allows to better understand the experimental results. Simulated force–displacement curves can be produced, and a fit procedure is helpful to compare these with the experimental results. It turns out that a model setup with a harder layer mimicking the extracellular matrix, where the model parameters are harder than in the rest of the body by a factor of 150, shows the best agreement with the experimental curves. This configuration shows a two-fold elastic behavior similar to the one observed in the experiments — unlike a configuration without an artificial extracellular matrix, whose force–displacement behavior is much closer to linear. This strain hardening coincides with the unfolding of the harder outside layer. Thus, in the numerical model the non-linear elastic behavior seems to be a geometric effect caused by an unfolding extracellular matrix.

Keeping in mind that the model setup with an extracellular matrix layer in neo-Hookean elasticity reproduces the measured force–displacement curves reasonably well and also mimics the unfolding behavior of the matrix, it seems probable that the elasticity of the wing disc tissue is also mainly governed by a geometric effect of a thin harder outer layer. Nevertheless, from our findings it cannot be excluded yet that three-dimensional effects play a significant role. Further work using a fully three-dimensional numerical deformation model based on a detailed surface reconstruction of the sample will hopefully explore these questions in the future.

7. Stress plots

See Figs. 8 and 9.

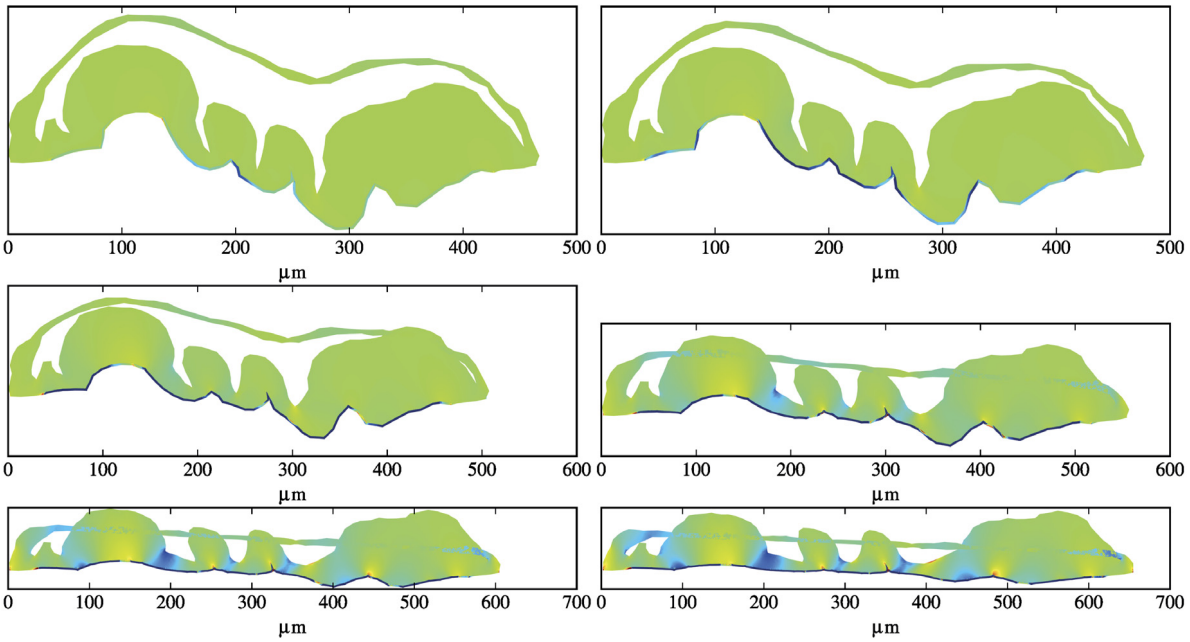

Fig. 9. Modeled deformation history: color coded is the vertical component σ_{yy} of the Cauchy stress tensor. The color scale varies from −0.04 MPa (blue) to 0.03 MPa (red). (For interpretation of the references to color in this figure legend, the reader is referred to the web version of this article.)

Acknowledgments

This work was funded by SystemsX.ch as part of the MorphogenetiX project as well as the Swiss National Science Foundation (SNF), Switzerland. The funders had no role in the design, analysis or publication of the research.

References

[1] see e.g. Nature Cell Biology focus series, May 31, 2017.
[2] M. Mittasch, P. Gross, M. Nestler, A.W. Fritsch, C. Iserman, M. Kar, M. Munder, A. Voigt, S. Alberti, S.W. Grill, M. Kreysing, Nature Cell Biol. 20 (2018) 344.
[3] V. Ruprecht, S. Wieser, A. Callan-Jones, M. Smutny, H. Morita, K. Sako, V. Barone, M. Ritsch-Marte, M. Sixt, R. Voituriez, C.P. Heisenberg, Cell 160 (2015) 673.
[4] J. Solon, A. Kaya-Copur, J. Colombelli, D. Brunner, Cell 137 (2009) 1331–1342.
[5] T. Lecuit, L. Le Goff, Nature 450 (2007) 189.
[6] S.J. Streichan, M. Lefebvre, N. Noll, E.F. Wieschaus, B.I. Shraiman, eLife Sci. 7 (2018) 27454.
[7] M. Rauzi, U. Krzic, T.E. Saunders, M. Krajnc, P. Ziherl, L. Hufnagel, M. Leptin, Nature Commun. 6 (2015) 8677.
[8] M. Behrndt, G. Salbreux, P. Campinho, R. Hauschild, F. Oswald, J. Roensch, S. Grill, C.P. Heisenberg, Science 338 (2012) 257.
[9] E. Farge, Curr. Biol. 13 (2003) 1365.
[10] D.E. Discher, et al., Science 324 (2009) 1673.
[11] B.I. Shraiman, Proc. Natl. Acad. Sci. USA 102 (2005) 3318.
[12] L. Hufnagel, A.A. Teleman, H. Rouault, S.M. Cohen, B.I. Shraiman, Proc. Natl. Acad. Sci. USA 104 (2007) 3835.
[13] T. Aegerter-Wilmsen, C.M. Aegerter, E. Hafen, K. Basler, MOD 124 (2007) 318.
[14] T. Aegerter-Wilmsen, et al., Development 139 (2012) 3221.
[15] T. Schluck, U. Nienhaus, T. Aegerter-Wilmsen, C.M. Aegerter, PLoSOne 8 (2013) e76171.
[16] Y. Pan, I. Heemskerk, C. Ibar, B.I. Shraiman, K.D. Irvine, Proc. Natl. Acad. Sci. USA 113 (2016) E6874.
[17] G.C. Fletcher, A. Elbediwy, I. Khanal, P.S. Ribeiro, N. Tapon, B.J. Thompson, EMBO J. 34 (2015) 940.
[18] T. Schluck, C.M. Aegerter, Eur. Phys. J. E 33 (2010) 111.
[19] S. Restrepo, J.J. Zartman, K. Basler, Methods Mol. Biol. 1478 (2016) 203.
[20] F. Lanfranconi, (Ph.D. thesis), Univ. of Zurich, 2017.
[21] R.S. Rivlin, Philos. Trans. R. Soc. Lond. A Math. Phys. Eng. Sci. 241 (835) (1948) 379–397.
[22] Y.C. Fung, in: Y.C. Fung, N. Perrone, M. Anliker (Eds.), Biomechanics: its Foundations and Objectives, Englewood Cliffs, Prentice-Hall, 1972.
[23] A. Logg, K.-A. Mardal, G. Wells, Automated Solution of Differential Equations By the Finite Element Method, Springer, 2012.